Real-time Local Stereo Matching Using Edge Sensitive Adaptive Windows

Maarten Dumont, Patrik Goorts, Steven Maesen, Philippe Bekaert and Gauthier Lafruit
Hasselt University - tUL - iMinds, Expertise Centre for Digital Media, Wetenschapspark 2, 3590 Diepenbeek, Belgium

Keywords: Stereo Matching, Adaptive Aggregation Windows, Real-time, Depth Estimation.

Abstract: This paper presents a novel aggregation window method for stereo matching, by combining the disparity hypothesis costs of multiple pixels in a local region more efficiently for increased hypothesis confidence. We propose two adaptive windows per pixel region, one following the horizontal edges in the image, the other the vertical edges. Their combination defines the final aggregation window shape that rigorously follows all object edges, yielding better disparity estimations with at least 0.5 dB gain over similar methods in literature, especially around occluded areas. Also, a qualitative improvement is observed with smooth disparity maps, respecting sharp object edges. Finally, these shape-adaptive aggregation windows are represented by a single quadruple per pixel, thus supporting an efficient GPU implementation with negligible overhead.

1 INTRODUCTION

3D entertainment systems, like 3D gaming with gesture recognition, 3DTV, etc. become increasingly popular. Such systems often benefit from extracting depth information by stereo matching instead of using active depth sensing methods, which introduce factors such as cost, indoor vs. outdoor lighting, sensitivity range, etc.

To this end, we present a stereo matching algorithm that provides improved disparity image quality by exploiting not only the vertical edges in the image, but also the horizontal edges, drastically improving its robustness over a range of applications.

Stereo matching uses a pair of images to estimate the apparent movement of the pixels from one image to the next. This apparent movement is more specifically known as the parallax effect, as demonstrated in Fig. 1, where two objects are shown, placed at different depths in front of a stereo pair of cameras. When moving from the left to the right camera view, an object undergoes a displacement – called the disparity – which is inversely proportional to the object's depth in the scene. Objects in the background (the palm tree) will have a smaller disparity in comparison to objects in the foreground (the blue buddy). The goal of stereo matching is to compute a dense disparity map by estimating each pixel's displacement.

There are typically 4 stages (Scharstein and Szeliski, 2002) in local dense stereo matching: cost calculation, cost aggregation, disparity selection, and refinement. Our method follows these stages, which is presented in an overview in Fig. 4.

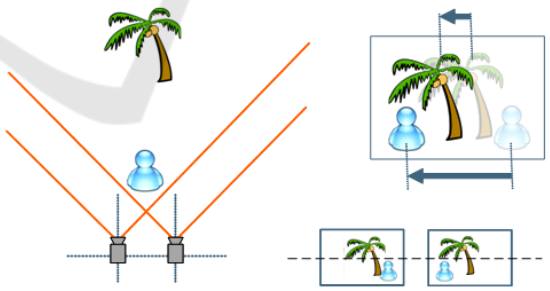

Figure 1: Concept of stereo vision. A scene is captured using 2 rectified cameras. Stereo matching attempts to estimate the apparent movement of the objects across the images. A large apparent movement (i.e. parallax) corresponds to close objects (a low depth value) and vice versa.

First, we consider each disparity and we calculate (in section 3) for each pixel in the left image the difference between that pixel and the corresponding pixel (based on the disparity under consideration) in the right image.

Our main contribution can be found in the aggregation step (in section 4), where the costs of neighboring pixels are taken into account to acquire the final cost. Previous methods typically use square windows (Scharstein and Szeliski, 2002), where the weight of each cost in the window can vary (Lu et al., 2007b). Alternatively, variable window sizes are used

Dumont M., Goorts P., Maesen S., Bekaert P. and Lafruit G..
Real-time Local Stereo Matching Using Edge Sensitive Adaptive Windows.
DOI: 10.5220/0005065301170126
In *Proceedings of the 11th International Conference on Signal Processing and Multimedia Applications* (SIGMAP-2014), pages 117-126
ISBN: 978-989-758-046-8

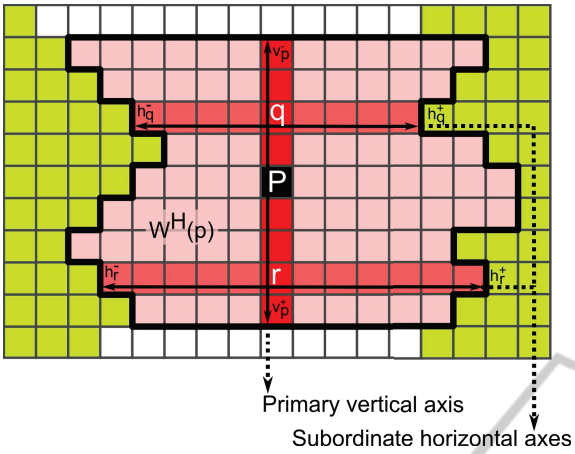

Figure 2: Derivation of the horizontal support window W^H using each pixel's axis-defining quadruple $(h_p^-, h_p^+, v_p^-, v_p^+)$.

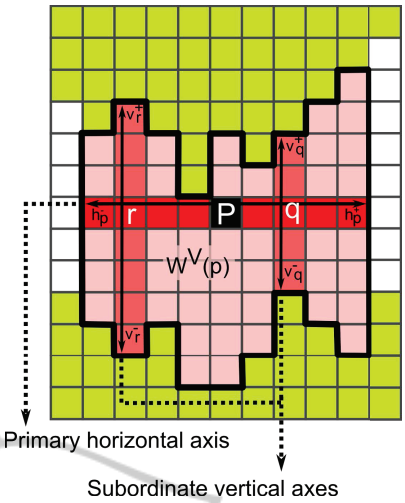

Figure 3: Derivation of the vertical support window W^V using each pixel's axis-defining quadruple $(h_p^-, h_p^+, v_p^-, v_p^+)$.

(Lu et al., 2007a), or the weights in the aggregation windows are adapted to the images (Richardt et al., 2010). In this paper, we use adaptive windows based on the color values in the input images, as an extension to the method of (Zhang et al., 2009a). We create two windows around the currently considered pixel, based on the color information in the images (section 2). We assume that pixels with similar colors belong to the same object, and therefore should get the same disparity value. One window grows in the horizontal direction and stops at edges; likewise the other window will grow in the vertical direction. Each window will favor a specific edge direction. Opposite to the method of (Zhang et al., 2009a), which uses only a horizontal window, we will combine these 2 directions, such that vertical edges are not favored.

Once the costs per pixel and per disparity are known, the most suitable disparity with the lowest cost is selected (in section 5) and the obtained disparity map is intelligently refined in three stages (in section 6).

Alternatively to local methods, global optimization methods based on graph cuts (and similar) (Yang et al., 2006; Wang et al., 2006; Papadakis and Caselles, 2010), segmented patches (Zitnick and Kang, 2007), and spatiotemporal consistency (Davis et al., 2003) are used that do not necessarily follow these steps.

To achieve high performance, we rely on parallel GPU computing by efficiently implementing in CUDA, which exposes the GPU as a massive SIMD architecture. Because of the specific nature of the hardware, our method achieves real-time performance. Results are presented in section 7, after which we conclude in section 8.

2 LOCAL SUPPORT WINDOWS

In the first step in our method, as shown in Fig. 4, we determine a suitable support window $W(p)$ for pixel p of the left image I. This window is used to aggregate the final cost for pixel p and should therefore be chosen carefully. To construct the window for a pixel p, we first determine a horizontal axis $\mathbb{H}(p)$ and vertical axis $\mathbb{V}(p)$ crossing in p. These 2 axes can be represented as a quadruple $\mathbb{A}(p)$:

$$\mathbb{A}(p) = (h_p^-, h_p^+, v_p^-, v_p^+) \tag{1}$$

where the component h_p^- represents how many pixels the horizontal axis extends on the left of p, v_p^+ represents how many pixels the vertical axis extends above p, and so forth. This is shown in Fig. 2 and Fig. 3.

To determine each component using color consistency, we keep extending an axis until the color difference between p and the outermost pixel q becomes too large, i.e.

$$\max_{c \in \{R,G,B\}} |I_c(p) - I_c(q)| \leq \tau \tag{2}$$

where $I_c(p)$ is color channel c of pixel p, and τ is the threshold for color consistency. We also stop extending if the size exceeds a maximum predefined size λ.

Using these 4 components, we define 2 local support windows for pixel p, referred to respectively as the horizontal local support window $W^H(p)$ and the vertical local support window $W^V(p)$.

Let's start by defining the horizontal window $W^H(p)$. First, we need to create its vertical axis based on the values of v_p^- and v_p^+. We call this the primary vertical axis $\mathbb{V}(p)$. Next, we consider the values of

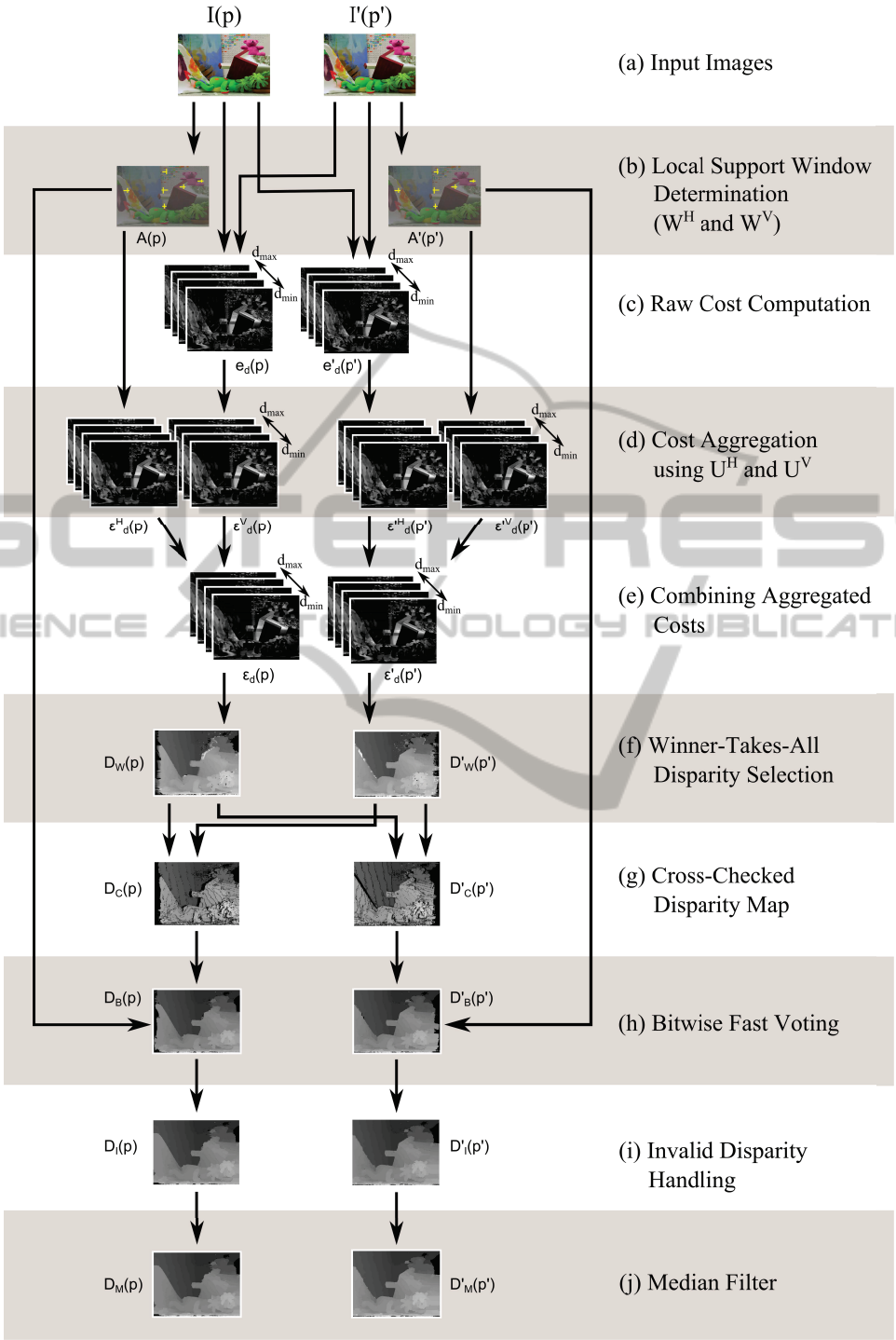

Figure 4: Overview of our method. (a) The input is a pair of rectified stereo images, in our case the standard Middlebury dataset Teddy (Scharstein and Szeliski, 2003) (b) First, we calculate the local support windows, based on color similarities in each image. (c) Next, we calculate the pixelwise cost per disparity. (d) These costs are aggregated, based on the support windows. There are 2 windows, and therefore 2 sets of aggregated costs. (e) The costs of the 2 windows are combined. (f) Next, we select the most suitable disparity value using a Winner-Takes-All approach. (g) A cross-check is performed to find any mismatches, typically caused by occlusions around edges. (h) The local support windows are used again to determine the most occurring disparity value in each window. This increases the quality of the disparity map. (i) Finally, any remaining invalid disparities are handled and (j) a median filter is applied to remove noise. The result is 2 disparity maps, one for each input image.

h_q^-, and h_q^+ for each pixel q on the primary vertical axis. These will define a horizontal axis per pixel q on the primary vertical axis. These axes are called the subordinate horizontal axes $\mathcal{H}(q)$. In short, this results in the orthogonal decomposition:

$$W^H(p) = \bigcup_{q \in \mathbb{V}(p)} \mathcal{H}(q) \tag{3}$$

An example is shown in Fig. 2.

Completely analogous but in the other direction, we define the vertical local support window $W^V(p)$ by creating a primary horizontal axis $\mathbb{H}(p)$ using h_p^-, and h_p^+, and on this axis create the subordinate vertical axes $\mathcal{V}(q)$:

$$W^V(p) = \bigcup_{q \in \mathbb{H}(p)} \mathcal{V}(q) \tag{4}$$

An example is shown in Fig. 3.

The support windows $W^H(p)$ and $W^V(p)$ will be used in the aggregation step, described in section 4. By requiring only the single quadruple $(h_p^-, h_p^+, v_p^-, v_p^+)$ to define both windows, we reduce memory usage, which is a serious consideration when doing GPU computing.

Using this method to define aggregation windows, we construct windows that are sensitive to edges in the image. The horizontal window $W^H(p)$ will fold nicely around vertical edges, because the width of each subordinate horizontal axis is variable. Horizontal edges are not followed as accurately, as the height of the window is fixed and only determined by its primary vertical axis. This situation, however, is reversed for $W^V(p)$. Thus by using both windows, we do not favor a single edge direction, which will yield better results.

Lastly, the notation $W'^H(p')$ and $W'^V(p')$ represents the local support windows for each pixel p' in the right image I'.

3 PER-PIXEL MATCHING COST

For a disparity hypothesis $d \in [d_{min}, d_{max}]$, consider the raw per-pixel matching cost $e_d(p)$, defined as the Sum of Absolute Differences (SAD):

$$e_d(p) = \frac{\sum_{c \in \{R,G,B\}} |I_c(p) - I'_c(p')|}{e_{max}} \tag{5}$$

where p is a pixel in the left image I with corresponding pixel p' in the right image I', and the coordinates of $p = (x_p, y_p)$ and $p' = (x'_{p'}, y'_{p'})$ relate to the disparity hypothesis d as $x'_{p'} = x_p - d$, $y'_{p'} = y_p$.

The constant e_{max} normalizes the cost $e_d(p)$ to the floating point range $[0,1]$. For example, when processing RGB images with 8 bits per channel, $e_{max} = 3 \times 255$.

We calculate $e_d(p)$ for each pixel p and refer to it as the per-pixel left confidence (or cost) map for disparity d. Similarly the per-pixel right confidence map can be constructed by calculating $e'_d(p')$ analogously to Eq. 5, with the x-coordinates of p and p' now related as $x_p = x'_{p'} + d$. The left and right per-pixel confidence maps for disparity $d = d_{min}$ are shown in Fig. 4(c).

4 COST AGGREGATION

For reliable cost aggregation, we symmetrically consider both local support windows $W(p)$ for pixel p in the left image and $W'(p')$ for pixel p' in the right image. If we only consider the local support window $W(p)$, the matching cost aggregation will be polluted by outliers in the right image, and vice versa. Therefore, while processing for disparity hypothesis d, the two local support windows are combined into what we will call a global support window $U_d(p)$. Distinguishing again between a horizontal and vertical global support window, they are defined as:

$$U_d^H(p) = W^H(p) \cap W'^H(p') \tag{6}$$

$$U_d^V(p) = W^V(p) \cap W'^V(p') \tag{7}$$

where the coordinates of $p = (x_p, y_p)$ and $p' = (x'_{p'}, y'_{p'})$ are again related to the disparity hypothesis d as $x'_{p'} = x_p - d$, $y'_{p'} = y_p$. In practice, this simplifies beautifully to taking the component-wise minimum of their axis quadruples from Eq. 1:

$$\mathbb{A}_d(p) = \min\left(\mathbb{A}(p), \mathbb{A}'(p')\right) \tag{8}$$

Two – more confident – matching costs $\varepsilon_d^H(p)$ and $\varepsilon_d^V(p)$ can now be aggregated over each pixel s of the horizontal and vertical global support windows $U_d^H(p)$ and $U_d^V(p)$ respectively:

$$\varepsilon_d^H(p) = \frac{1}{\left\|U_d^H(p)\right\|} \sum_{s \in U_d^H(p)} e_d(s) \tag{9}$$

$$\varepsilon_d^V(p) = \frac{1}{\left\|U_d^V(p)\right\|} \sum_{s \in U_d^V(p)} e_d(s) \tag{10}$$

where the number of pixels $\|U_d(p)\|$ in the support window acts as a normalizer. These aggregated confidence maps are shown in Fig. 4(d) for disparity hypothesis $d = d_{min}$.

We next propose 2 methods to select the final aggregated cost $\varepsilon_d(p)$, based on $\varepsilon_d^H(p)$ and $\varepsilon_d^V(p)$. The first method takes the minimum and assumes that the lowest cost will actually be the correct solution:

$$\varepsilon_d(p) = \min\left(\varepsilon_d^H(p), \varepsilon_d^V(p)\right) \tag{11}$$

The second method uses a weighted sum and is more robust against errors in the matching process:

$$\varepsilon_d(p) = \alpha\,\varepsilon_d^H(p) + (1-\alpha)\,\varepsilon_d^V(p) \tag{12}$$

where α is a weighting parameter between 0 and 1.

Again this combined confidence map is shown in Fig. 4(e).

The aggregation is repeated over the right image, in order to arrive at a left and right aggregated confidence map. This means computing $\mathbb{A}'_d(p') = \min(\mathbb{A}(p), \mathbb{A}'(p'))$, with p and p' now related as $x_p = x'_{p'} + d$ and from there setting up an analogous reasoning to end up at $\varepsilon'_d(p')$.

4.1 Fast Cost Aggregation Using Orthogonal Integral Images

From the global axis quadruple $\mathbb{A}_d(p)$ of Eq. 8 and following the same reasoning that defined the local support windows in section 2, an orthogonal decomposition of the global support windows $U_d^H(p)$ and $U_d^V(p)$ can be obtained, analogous to Eq. 3 and Eq. 4:

$$U_d^H(p) = \bigcup_{q \in \mathbb{V}_d(p)} \mathcal{H}_d(q) \tag{13}$$

$$U_d^V(p) = \bigcup_{q \in \mathbb{H}_d(p)} \mathcal{V}_d(q) \tag{14}$$

This orthogonal decomposition is key to a fast and efficient implementation of the cost aggregation step. Substituting Eq. 13 into Eq. 9 and Eq. 14 into Eq. 10, we separate the inefficient $\sum_{s \in U_d(p)} e_d(s)$ into a horizontal and vertical integration (Zhang et al., 2009a):

$$\varepsilon_d^H(p) = \sum_{q \in \mathbb{V}_d(p)} \left(\sum_{s \in \mathcal{H}_d(q)} e_d(s) \right) \tag{15}$$

$$\varepsilon_d^V(p) = \sum_{q \in \mathbb{H}_d(p)} \left(\sum_{s \in \mathcal{V}_d(q)} e_d(s) \right) \tag{16}$$

where the normalizer $\frac{1}{\|U_d(p)\|}$ has been omitted for clarity.

For the global horizontal support window $U_d^H(p)$, Eq. 15 intuitively means to first aggregate costs over its subordinate horizontal axes $\mathcal{H}_d(q)$ and then over its primary vertical axis $\mathbb{V}_d(p)$. Vice versa for the vertical configuration of $U_d^V(p)$ in Eq. 16.

5 DISPARITY SELECTION

After the left and right aggregated confidence maps from section 4 have been computed for every disparity $d \in [d_{min}, d_{max}]$, the best disparity per pixel (i.e. the one with lowest cost $\varepsilon_d(p)$) is selected using a Winner-Takes-All approach:

$$D_W(p) = \underset{d \in [d_{min}, d_{max}]}{\arg\min}\ \varepsilon_d(p) \tag{17}$$

which results in the initial disparity maps $D_W(p)$ for the left image and $D'_W(p')$ for the right image, both shown in Fig. 4(f).

At the same time we also keep a final horizontally and vertically aggregated confidence map:

$$\varepsilon^H(p) = \min_{d \in [d_{min}, d_{max}]} \varepsilon_d^H(p) \tag{18}$$

$$\varepsilon^V(p) = \min_{d \in [d_{min}, d_{max}]} \varepsilon_d^V(p) \tag{19}$$

Next we cross-check the disparities between the two initial disparity maps for consistency. A left-to-right cross-check of the left disparity map $D_W(p)$ means that for each of its pixels p, the corresponding pixel p' is determined in the right image based on the disparity $D_W(p)$, and the disparity $D'_W(p')$ in the right disparity map is compared to $D_W(p)$. If they differ, the cross-check fails and the disparity is marked as invalid:

$$D_C(p) = \begin{cases} D_W(p) & \text{if } D_W(p) = D'_W(p') \\ \textit{INVALID} & \text{elsewhere} \end{cases} \tag{20}$$

where p is now related to p' as $x'_{p'} = x_p - D_W(p)$, $y'_{p'} = y_p$. The process is then reversed for a right-to-left cross-check of the disparity map $D'_W(p')$, which leaves us with the left and right cross-checked disparity maps $D_C(p)$ and $D'_C(p')$ to be refined in section 6.

Invalid disparities are most likely to occur around edges in the image, where occlusions are present in the scene. In Fig. 4(g) we show these occluded regions as pure black (marked as invalid) pixels.

6 DISPARITY REFINEMENT

We refine the disparity maps found in the previous section in three stages, (h) to (j) in Fig. 4.

First, the local support windows as described in section 2 can be employed again, to update a pixel's disparity with the disparity that appears most inside

its windows. This method is the most powerful and is detailed in section 6.1.

Next, any remaining invalid disparities are handled in section 6.2.

Finally, the disparity map is filtered using a 3×3 median filter to remove any remaining speckle noise in section 6.3.

6.1 Bitwise Fast Voting over Local Support Windows

In this first stage of the refinement we will update a pixel's disparity with the disparity that is most present inside its local support windows W^H and W^V as defined in section 2. We may say that this refinement is valid, because pixels in the same window have similar colors by definition, and therefore with high probability belong to the same object and should have the same disparity. Confining the search to the local support windows also ensures that we greatly reduce the risk of edge fattening artifacts.

To efficiently determine the most frequent disparity value within a support window, we apply a technique called Bitwise Fast Voting by (Zhang et al., 2009b) and adapt it to handle both horizontally and vertically oriented support windows. At the core of the Bitwise Fast Voting technique lies a procedure that derives each bit of the most frequent disparity independently from the other bits. It is however reasonable to assume this is valid (Zhang et al., 2009b).

First consider a pixel p with local support window $W(p)$. We sum the lth bit $b_l(s)$ (either 0 or 1) of the disparity value $D_C(s)$ of all pixels s in the support window, and call the result $B_l(p)$. Furthermore distinguishing between horizontal and vertical support windows, this gives:

$$B_l^H(p) = \sum_{s \in W^H(p)} b_l(s) \tag{21}$$

$$B_l^V(p) = \sum_{s \in W^V(p)} b_l(s) \tag{22}$$

The lth bit $D_B^l(p)$ of the final disparity value $D_B(p)$ is then decided as:

$$D_B^l(p) = \begin{cases} 1 & \text{if } B_l(p) > \beta \times N(p) \\ 0 & \text{elsewhere} \end{cases} \tag{23}$$

where $\beta \in [0,1]$ is a parameter that we will come back to below.

This leaves us to determine exactly what $B_l(p)$ and $N(p)$ in Eq. 23 are. For this we again propose two methods. The first method is similar to Eq. 11 and relies on the minimum between the horizontally and vertically aggregated confidence maps $\varepsilon^H(p)$ (Eq. 18) and $\varepsilon^V(p)$ (Eq. 19):

$$B_l(p) = \begin{cases} B_l^H(p) & \text{if } \varepsilon^H(p) \leq \varepsilon^V(p) \\ B_l^V(p) & \text{elsewhere} \end{cases} \tag{24}$$

$$N(p) = \begin{cases} \left\|W^H(p)\right\| & \text{if } \varepsilon^H(p) \leq \varepsilon^V(p) \\ \left\|W^V(p)\right\| & \text{elsewhere} \end{cases} \tag{25}$$

The second method uses a weighted sum:

$$B_l(p) = \alpha\, B_l^H(p) + (1-\alpha)\, B_l^V(p) \tag{26}$$

$$N(p) = \alpha \left\|W^H(p)\right\| + (1-\alpha) \left\|W^V(p)\right\| \tag{27}$$

where α is as in Eq. 12.

To recap, for a pixel p, Eq. 23 says that the lth bit of its final disparity value is 1 if the lth bit appears as 1 in most of the disparity values under its local support window. The number of actual 1 appearances are counted in $B_l(p)$, whereas the maximum possible appearances of 1 is represented by the window size $N(p)$. The sensitivity parameter β controls how many appearances of 1 are required to confidently vote the result and is best set to 0.5.

It is important to note that certain disparities might be invalid due to the cross-check of $D_C(p)$ in section 5. While counting bit votes, we must take this into account by reducing $N(p)$ accordingly. This way the algorithm is able to update an invalid disparity by depending on votes from valid neighbors, and thereby reliably fill in occlusions and handle part of the image borders. The improvement in quality that this method yields in the disparity maps is already very apparent from the visual difference between Fig. 4(f) and Fig. 4(h).

A couple of key observations make that this method is called fast. First, the number of iterations needed to determine every bit of the final disparity value is limited by d_{max}. For example, in the Middlebury Teddy scene we use $d_{max} = 53$, which represents binary as 110101, and thus only 6 iterations suffice. Furthermore, the votes can be counted very efficiently by orthogonally separating Eq. 21 and Eq. 22, analogously to Eq. 15 and Eq. 16. All this results in high efficiency with low memory footprint.

6.2 Invalid Disparity Handling

The Bitwise Fast Voting technique from the previous section 6.1 removes many of the invalid disparity values by applying the most occurring valid value inside its windows. However, this will fail if the window does not contain any valid values, or in other words,

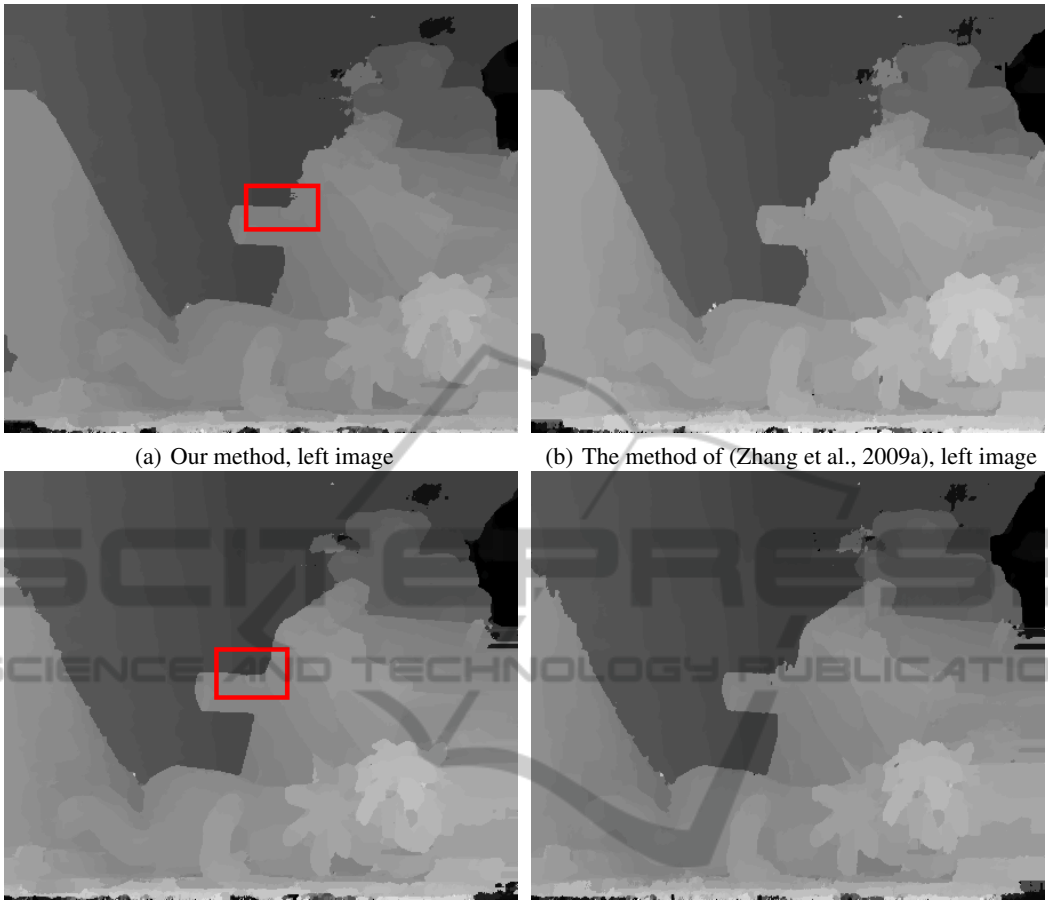

(a) Our method, left image (b) The method of (Zhang et al., 2009a), left image

(c) Our method, right image (d) The method of (Zhang et al., 2009a), right image

Figure 5: Comparison of our method (a), (c) and the similar method of (Zhang et al., 2009a)(b), (d), for both the left and right images. The results clearly show that the edges in the image are more correct and contain less artifacts. This is especially true for horizontal edges, as highlighted by the red squares.

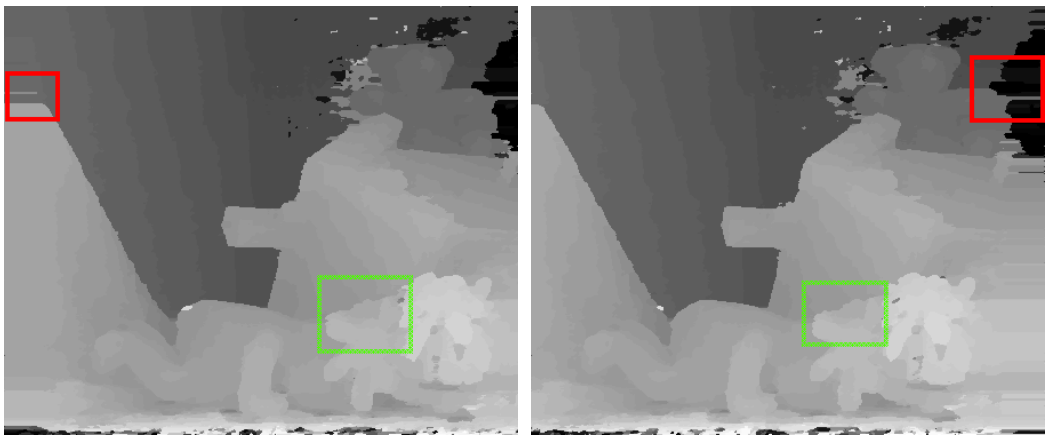

(a) Without bitwise fast voting, left image (b) Without bitwise fast voting, right image

Figure 6: Results without bitwise voting. The results with bitwise voting are shown in Figure 5, (a) and (c). The red, full squares show the result at the borders of the disparity maps. Not enough information is available in both images to estimate the disparity correctly. Therefore, filling these values naively will result in erroneous lines. By using bitwise voting, these artifacts are eliminated. The green, dashed squares show the handling of invalid disparity values around edges in the images (i.e. occlusion). When no bitwise voting is applied, edges are fattened and the disparity values *leak* over the edges, resulting in artifacts. This is avoided by incorporating color information.

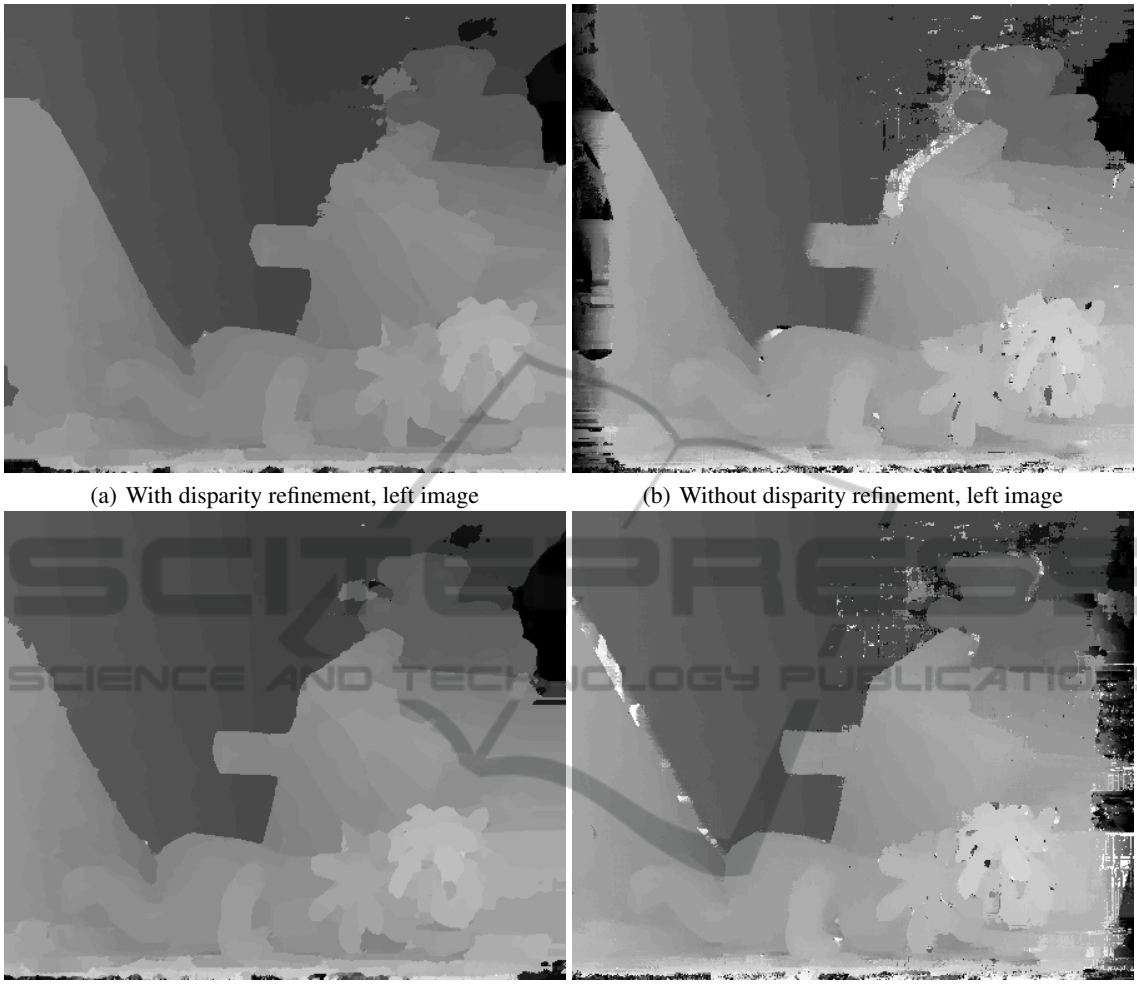

(a) With disparity refinement, left image (b) Without disparity refinement, left image

(c) With disparity refinement, right image (d) Without disparity refinement, right image

Figure 7: Comparison of the results with and without disparity refinement. Many artifacts are eliminated, including errors at the borders of the disparity maps, speckle noise, mismatches that only occur in one disparity map, etc.

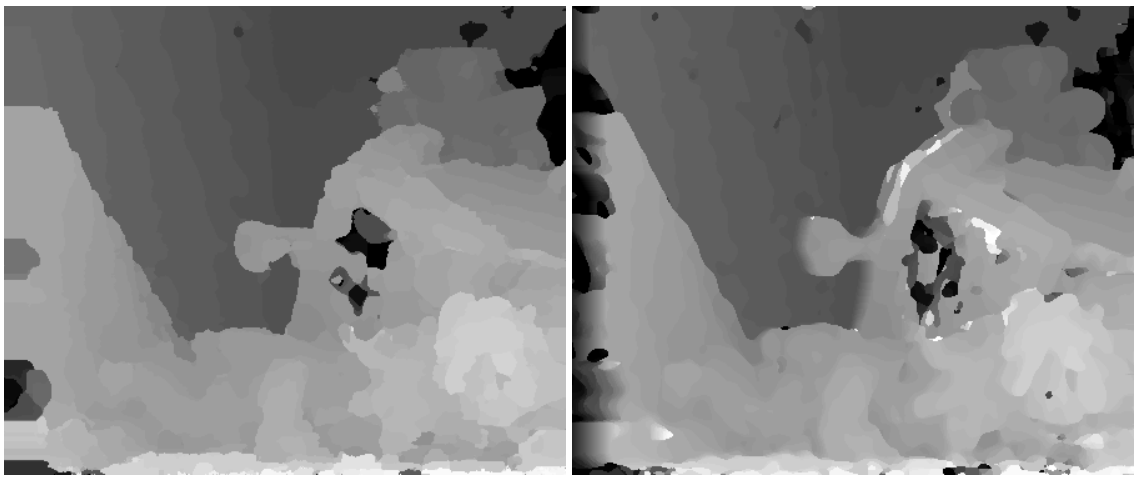

(a) With bitwise fast voting (b) Without bitwise fast voting

Figure 8: Comparison of the results with and without bitwise voting for stereo methods using fixed square aggregation windows. The results are clearly better when applying bitwise voting. This demonstrates that this method is not only applicable to the aggregation windows described above.

when $N(p) = 0$ (Eq. 23). This occurs mostly near the borders of the disparity maps, but can also manifest itself anywhere in the image where the occlusions are large enough.

We will therefore estimate a value for the remaining invalid disparities, and store them in the corrected disparity map $D_I(p)$. For each pixel with an invalid disparity value, we search to the left and to the right on its scanline for the closest valid disparity value. The disparity map is not updated iteratively, so that only the information of $D_B(p)$ is used for each pixel. The result is shown in Fig. 4(i).

6.3 Median Filter

In the last refinement step, small disparity outliers are filtered using a median filter, resulting in the absolute final disparity map $D_M(p)$ shown in Fig. 4(j). A median filter has the property of removing speckle noise, in this case caused by disparity mismatches, while returning a sharp signal (unlike an averaging filter). In our method, we calculate the median for each pixel over a 3×3 window using a fast bubble sort (Astrachan, 2003) implementation in CUDA.

7 RESULTS

We demonstrate the effectiveness of our method using the standard Middlebury dataset Teddy (Scharstein and Szeliski, 2003). We compare our method with the method of (Zhang et al., 2009a), which only uses a horizontal primary axis, using our own implementation to provide a valid comparison. All comparisons with ground truth data use the PSNR metric, where higher is better.

Our method is better with an increase of 0.53 dB, i.e. from 18.65 dB to 19.18 dB. Furthermore, the results are visually better, as observed in Fig. 5. The figure clearly shows that the edges in the image contain less artifacts, especially around horizontal edges.

As we will discuss next, the refinement steps of section 6 contribute significantly to the final quality of the disparity maps, which show significant improvements both visually and quantitatively measured by the PSNR metric.

Fig. 6 shows the result when the bitwise fast voting is disabled. Here, all invalid disparity values are handled by using the closest value on the pixel's scanline. We make two observations. First, the borders of the disparity maps show a clear decrease in quality. This is caused by the fact that many invalid disparity values can be found here due to the missing information in one of the images. Because using the closest valid disparity value does not take the color values into account, artifacts are created. Second, edge fattening, meaning that the disparity values *leak* over the edges, can be seen everywhere in the image. Again, this is because no color information is used to estimate the invalid disparity values. The use of bitwise voting gives an increase of 0.75 dB, from 18.43 dB to 19.18 dB.

Finally, Fig. 7 shows the result when no refinement is applied at all. Many improvements can be noticed visually, including the elimination of speckle noise, errors at the borders of the disparity map, etc. Compared to the ground truth, we demonstrate an improvement of 3.52 dB, from 15.66 dB to 19.18 dB.

As a matter of fact, bitwise voting can be applied to any local stereo algorithm. To demonstrate this, we applied bitwise voting to a disparity map that was computed using fixed square aggregation windows. This is shown in Fig. 8. As shown, the results improve, but all artifacts from a naive stereo matching algorithm cannot be eliminated.

Our method runs at 13 FPS for 450×375 resolution images on an NVIDIA GTX TITAN, therefore providing a real-time solution.

8 CONCLUSION

We have shown that combining horizontal and vertical edge aggregation windows in stereo matching yields high quality levels in the disparity map estimation. A 0.5 dB gain over state-of-the-art methods and smooth disparity images with sharp edge preservation around objects is achieved. Nonetheless, the complexity of the final solution is comparable to existing methods, allowing efficient GPU implementation. Furthermore, we demonstrate that the disparity refinement has a large effect on the final quality.

REFERENCES

Astrachan, O. (2003). Bubble sort: an archaeological algorithmic analysis. *ACM SIGCSE Bulletin*, 35(1):1–5.

Davis, J., Ramamoorthi, R., and Rusinkiewicz, S. (2003). Spacetime stereo: A unifying framework for depth from triangulation. In *Computer Vision and Pattern Recognition, 2003. Proceedings. 2003 IEEE Computer Society Conference on*, volume 2, pages II–359. IEEE.

Lu, J., Rogmans, S., Lafruit, G., and Catthoor, F. (2007a). High-speed dense stereo via directional center-biased support windows on programmable graphics hardware. In *Proceedings of 3DTV-CON: The True Vision Capture, Transmission and Display of 3D Video*, Kos, Greece.

Lu, J., Rogmans, S., Lafruit, G., and Catthoor, F. (2007b). Real-time stereo using a truncated separable laplacian kernel approximation on programmable graphics hardware. In *Proceedings of International Conference on Multimedia and Expo*, pages 1946–1949, Beijing, China.

Papadakis, N. and Caselles, V. (2010). Multi-label depth estimation for graph cuts stereo problems. *Journal of Mathematical Imaging and Vision*, 38(1):70–82.

Richardt, C., Orr, D., Davies, I., Criminisi, A., and Dodgson, N. A. (2010). Real-time spatiotemporal stereo matching using the dual-cross-bilateral grid. In *Computer Vision–ECCV 2010*, pages 510–523. Springer.

Scharstein, D. and Szeliski, R. (2002). A taxonomy and evaluation of dense two-frame stereo correspondence algorithms. *International journal of computer vision*, 47(1):7–42.

Scharstein, D. and Szeliski, R. (2003). High-accuracy stereo depth maps using structured light. In *Proceedings of the IEEE Conference on Computer Vision and Pattern Recognition (CVPR 2003)*, volume 1, pages 195–202. IEEE.

Wang, L., Liao, M., Gong, M., Yang, R., and Nister, D. (2006). High-quality real-time stereo using adaptive cost aggregation and dynamic programming. In *3D Data Processing, Visualization, and Transmission, Third International Symposium on*, pages 798–805. IEEE.

Yang, Q., Wang, L., Yang, R., Wang, S., Liao, M., and Nister, D. (2006). Real-time global stereo matching using hierarchical belief propagation. In *BMVC*, volume 6, pages 989–998.

Zhang, K., Lu, J., and Lafruit, G. (2009a). Cross-based local stereo matching using orthogonal integral images. *Circuits and Systems for Video Technology, IEEE Transactions on*, 19(7):1073–1079.

Zhang, K., Lu, J., Lafruit, G., Lauwereins, R., and Van Gool, L. (2009b). Real-time accurate stereo with bitwise fast voting on cuda. In *Computer Vision Workshops (ICCV Workshops), 2009 IEEE 12th International Conference on*, pages 794–800. IEEE.

Zitnick, C. L. and Kang, S. B. (2007). Stereo for image-based rendering using image over-segmentation. *International Journal of Computer Vision*, 75(1):49–65.